J. Fluid Mech. (1989), *vol.* 201, *pp.* 123–146
Printed in Great Britain

A theoretical study of the motion of a viscous drop toward a fluid interface at low Reynolds number

By B. K. CHI† AND L. G. LEAL‡

† Aerojet General Corp., Tustin, CA 92680, USA

‡ Department of Chemical Engineering, California Institute of Technology, Pasadena, CA 91125, USA

(Received 20 April 1987 and in revised form 1 August 1988)

In this paper we use a boundary-integral technique to numerically investigate the motion of a viscous drop toward a fluid–fluid interface at low Reynolds number. We consider only the case of a drop moving toward its homophase. The solutions include large deformations of both the drop and interface for capillary numbers in the range $0.2 \leqslant Ca \leqslant 10$ and the viscosity ratios between $0.1 \leqslant \lambda \leqslant 10$, and illustrate the approach toward a film-drainage geometry for a drop which starts at a large distance from an initially undeformed, flat interface. We also consider briefly the effect of starting the drop closer to the interface.

1. Introduction

The dynamics of a droplet rising through an immiscible fluid toward a horizontal interface has been studied frequently, via both experimental and theoretical investigations. Interest in the problem is primarily because of its role as a simple model problem for coalescence. Three distinct cases can be identified: one in which the drop and the fluid on the other side of the interface are the same (in this case, the drop is said to coalesce with its homophase); the second where the fluid across the interface is not the same as the drop, but the drop is nevertheless miscible in it; and the third case in which all three fluids are different and immiscible. The present study is concerned with the first of these cases, though the governing equations are initially posed for the most general case, the third, in anticipation of future analysis.

In the case when fluid 1 is the same as fluid 3 (see figure 1), coalescence occurs via a film-drainage mechanism, and earlier studies have focused completely on the dynamics of the film-drainage step. In principle, this makes the theoretical problem much simpler because the assumption of a thin film allows a lubrication-type analysis at the leading order of approximation, but knowledge of an initial film shape is required, and this generally must come from the dynamics that occur prior to the lubrication regime. Many theoretical papers have been published that analyse the dynamics of film drainage (cf. Charles & Mason 1960; Frankel & Mysels 1962; Princen 1963), including calculation of the shape of the film (Burrill & Woods 1969, 1973; Hartland 1970; Jones & Wilson 1978), calculation of the effects of interface immobility due to surfactant or other mechanisms (Princen 1963; Lin & Slattery 1982), and the effect of London–van der Waals forces (Chen, Hahn & Slattery 1984). In addition, many experimental investigations of film dynamics have also been reported – frequently with the drop formed and released very near to the interface. Allen, Charles & Mason (1961), MacKay & Mason (1963) and Princen & Mason (1965) used a light interference technique to measure the film thickness, and the dynamics

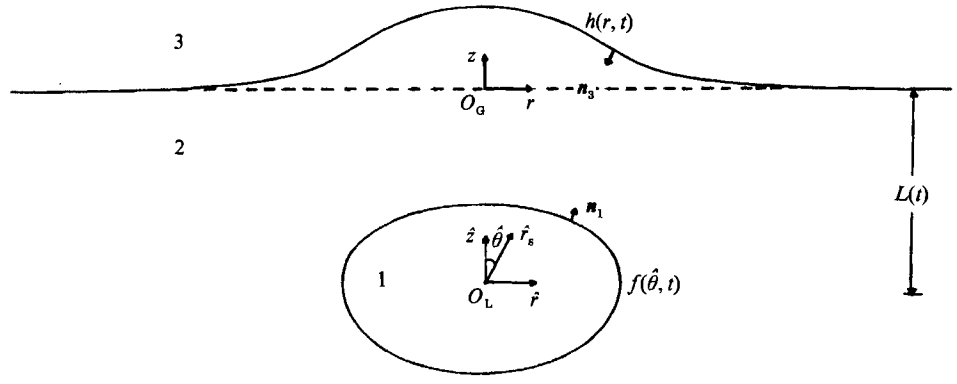

FIGURE 1. Description of the coordinate system; O_L: origin of the local (spherical) coordinate system; O_G: origin of the global (cylindrical) coordinate system.

of the drainage process, while Hartland (1967*a–d*, 1969) used a capacitance technique for the same purpose, and also presented photographs of overall shapes of the drop near the interface. Hodgson & Woods (1969) and Burrill & Woods (1973) later adopted the light interference technique to study the influence of controlled additions of surfactant on film drainage.

Although the literature is thus crowded with studies of the film-drainage step of the coalescence process, it is not clear that a complete picture actually results. In all cases, the shape of the interfaces (and film) must depend upon the initial conditions (or shape at some earlier moment in time). But, experimentally, films have often been established by initially placing a drop very close to an interface, and it is not obvious how the resulting film relates to that which would occur if the drop had been released at a larger distance from the interface. From the theoretical point of view, an initial film profile (shape) must be specified – most often this is simply taken from an experimental observation at some time, t_0, and the theoretically predicted shapes at later times are then compared with observed shapes for the same initial configuration. But little emphasis has been placed on the dynamics of the processes which lead to the thin-film geometry, or on the dependence of the initial film configuration on independent parameters, such as Reynolds number, capillary number or viscosity ratio. The solution procedure of Lin & Slattery (1982), and later of Chen *et al.* (1984) does avoid the necessity for input of an empirical initial state, but only at the cost of a large number of *ad hoc* assumptions. The most successful analysis of this type is due to Jones & Wilson (1978), but their theory still requires the severe assumption of a quasi-static configuration. Almost all of the preceding theories have also analysed motion only in the thin film, with either zero tangential stress ('mobile' interface) or no-slip ('immobile' interface) conditions prescribed at both the drop surface and the interface between the two bulk fluids (exceptions are Reed, Riolo & Hartland 1974*a*, *b*; Riolo & Hartland 1975; Jones & Wilson 1978; Chen *et al.* 1984; and Hahn & Slattery 1985, 1986). With these boundary conditions, it is not possible to assess the role of the physical properties of the drop or the second bulk fluid, nor can any physico–chemical effect be considered which involves mass transport in these fluids. Many of these limitations of film theories are a consequence of the well-known fact that the lubrication approximation describes only the first term of an asymptotic series for one part of the flow domain. Without matching to

connect the film analysis to the overall drop shape and the flow in other parts of the domain, it is not possible to establish conditions, in terms of either fluid/interface properties or the prior history of drop and interface shape and motion, when a particular version of the film theory will represent an adequate local approximation to the overall solution.

In the present paper, we adopt a complementary approach that involves solution of the complete fluid-mechanics problem, for the limiting case of small inertia ($Re \ll 1$). The solution of free-boundary problems at zero Reynolds numbers via the so-called 'boundary-integral' technique has by now become a routine and inexpensive means to investigate phenomena such as coalescence, with no need for simplifying approximations (and resultant limitations) such as those inherent in the film-drainage, lubrication limit. Thus, for example, Lee & Leal (1982) and Geller, Lee & Leal (1986) have recently used the boundary-integral technique to study the motion of a rigid sphere toward an initially flat, but deformable interface, with the qualitatively important result of identifying two distinct modes of deformation and breakthrough – one corresponding to 'film drainage' and the other to the formation of a highly deformed interface in which the sphere carries a layer of the original fluid with it across the original plane of the interface, until 'breakthrough' eventually occurs by pinch-off of a 'tail' behind the sphere. The present paper reports on the initial phase of a complementary study of the motion of a deformable drop toward an initially flat interface, for the important case in which the drop and the second fluid are the same. In this case, the drop ultimately moves very slowly, and a thin-film configuration is achieved. However, we consider the 'complete' fluid-mechanics problem, starting with the drop at some finite distance from the interface, and including motion both within the drop and in the upper bulk fluid. A primary goal is to examine the role of interfacial tension (capillary number), and of the viscosity ratio in determining the interface and drop shapes, and thus the 'shape' of the thin film.

In the present work, we consider only interfacial, viscous and gravitational forces. London–van der Waals and electrostatic forces will become significant when the film is $O(1000$ Å) in thickness, and are likely to be responsible for the film 'instability' that finally leads to coalescence, but they are not considered here. The interface is also assumed to be 'clean' and thereby characterized completely by a constant value of interfacial tension. The motion, plus interface and drop shapes, are constrained to be axisymmetric.

2. Problem statement

We consider a drop of a light liquid (fluid 1) rising through an immiscible heavy liquid (fluid 2), toward an initially flat interface which separates the heavy bulk fluid (fluid 2) and another lighter bulk fluid (fluid 3), as indicated in figure 1. All fluids are incompressible and Newtonian. The interfaces between fluids 1 and 2, and 2 and 3 are both assumed to be clean, mobile, and characterized completely by constant interfacial tensions, denoted respectively as γ_{12} and γ_{23}. In the calculations reported later in this paper, we shall restrict our attention to systems for which the drop and the upper fluid are the same, i.e. fluid 1 = fluid 3. Here, however, we initially formulate the problem for the general three-fluid system. The governing equations and boundary conditions are identical for a heavy drop falling toward the interface from above.

We assume that the creeping-motion approximation is applicable to the motion of the drop, and thus neglect all inertia effects. The resulting solutions are therefore valid when

$$Re = \frac{u_c l_c \rho_2}{\mu_2} \ll 1. \tag{1}$$

A convenient choice for l_c is the undeformed drop radius a, and a conservative choice for u_c is the velocity of a spherical drop of fluid 1 in an unbounded fluid 2 (hereafter denoted as U_∞). Since the drop moves as a consequence of buoyancy,

$$U_\infty = \frac{2}{9}\frac{ga^2(\rho_2-\rho_1)}{\mu_2}\frac{1}{\beta}, \tag{2}$$

where $$\beta = \left(1+\frac{2}{3\lambda_1}\right)\Big/\left(1+\frac{1}{\lambda_1}\right), \qquad \lambda_1 = \frac{\mu_1}{\mu_2}.$$

This characteristic velocity is an upper bound on the actual velocity of the drop, which decreases from (2) as the drop approaches the interface.

The governing differential equations in dimensionless form are then

$$-\nabla p_1 + \lambda_1 \nabla^2 \boldsymbol{u}_1 = 0, \quad \nabla \cdot \boldsymbol{u}_1 = 0 \quad \text{for fluid 1,} \tag{3}$$

$$-\nabla p_2 + \nabla^2 \boldsymbol{u}_2 = 0, \quad \nabla \cdot \boldsymbol{u}_2 = 0 \quad \text{for fluid 2,} \tag{4}$$

$$-\nabla p_3 + \lambda_3 \nabla^2 \boldsymbol{u}_3 = 0, \quad \nabla \cdot \boldsymbol{u}_3 = 0 \quad \text{for fluid 3,} \tag{5}$$

in which the characteristic pressure is taken as

$$p_c \equiv \frac{\mu_2 U_\infty}{a},$$

and $\lambda_1 \equiv \mu_1/\mu_2, \lambda_3 \equiv \mu_3/\mu_2$.

We formulate the problem in a laboratory frame of reference in which the drop moves with velocity U through a fluid that is stationary far from the drop, i.e.

$$\boldsymbol{u}_2, \boldsymbol{u}_3 \to 0 \quad \text{as} \quad |\boldsymbol{x}| \to \infty. \tag{6}$$

On the interface separating fluids 2 and 3, $\boldsymbol{x} \in S_1$, we require

$$\boldsymbol{u}_2 = \boldsymbol{u}_3, \tag{7}$$

$$\boldsymbol{n}_3 \cdot \boldsymbol{T}_2 - \lambda_3 \boldsymbol{n}_3 \cdot \boldsymbol{T}_3 = \boldsymbol{n}_3 \frac{1}{Ca_3} \nabla \cdot \boldsymbol{n}_3 - \frac{1}{Cg_3} h \boldsymbol{n}_3, \tag{8}$$

$$\boldsymbol{n}_3 \cdot \boldsymbol{u}_2 = \boldsymbol{n}_3 \cdot \boldsymbol{u}_3 = \frac{1}{|\nabla H|}\frac{\partial h}{\partial t}. \tag{9}$$

In these equations, the interface is conveniently specified using a cylindrical coordinate system as $z = h(r,t)$, where z is normal to the plane of the undeformed interface (it is convenient to specify this plane as $z = 0$), and r is the radial distance from the axis of symmetry. The vector $\boldsymbol{n}_3$ is the unit normal into fluid 2 at the interface, i.e. $\boldsymbol{n}_3 = -\nabla H/|\nabla H|$ with $H = z - h(r,t)$, as shown in figure 1.

Equation (9) is the kinematic condition that relates the normal velocity components at the interface to the rate of displacement of the interface above the undisturbed plane, $z = 0$. Equation (8) is the surface stress condition, and contains both continuity of tangential stress, and the normal stress balance between viscous and pressure stresses, and capillary and body forces. The parameter

Ca_3 is the capillary number, $Ca_3 \equiv \mu_2 U_\infty/\gamma_{23}$, and Cg_3 is the body force parameter, $Cg_3 \equiv \mu_2 U_\infty/ga^2(\rho_2-\rho_3)$. The body force terms appear in (8) because the equations of motion are written in terms of the dynamic pressure; i.e. the stress $\boldsymbol{T}_i$ in (8) is the total stress minus the hydrostatic pressure contribution.

In addition to (6)–(9), boundary conditions must also be applied at the drop surface, $\boldsymbol{x} \in S_D$. These can be expressed in the form

$$\boldsymbol{u}_1 = \boldsymbol{u}_2, \tag{10}$$

$$\boldsymbol{n}_1 \cdot \boldsymbol{T}_2 - \lambda_1 \boldsymbol{n}_1 \cdot \boldsymbol{T}_1 = \frac{1}{Ca_1}(\nabla \cdot \boldsymbol{n}_1)\boldsymbol{n}_1 - \frac{1}{Cg_1}(-L + f\cos\hat{\theta})\boldsymbol{n}_1, \tag{11}$$

$$\boldsymbol{n}_1 \cdot \left(\boldsymbol{u}_1 + \frac{\partial L}{\partial t}\boldsymbol{i}_z\right) = \boldsymbol{n}_1 \cdot \left(\boldsymbol{u}_2 + \frac{\partial L}{\partial t}\boldsymbol{i}_z\right) = \frac{1}{|\nabla F|}\frac{\partial f}{\partial t}. \tag{12}$$

Again, these are continuity of velocity, the surface stress condition, and the kinematic condition.

The kinematic condition (12) relates the rate of change of the drop shape to the normal velocity components at its surface. The most convenient way to specify the drop is to specify its radial dimension, as a function of the polar angle $\hat{\theta}$ shown in figure 1, relative to its centre of mass. In this case, the drop surface is given as

$$F(\hat{r}_s, \hat{\theta}, t) \equiv \hat{r}_s - f(\hat{\theta}, t) = 0, \tag{13}$$

where $(\hat{r}_s, \hat{\theta})$ are components of a local spherical coordinate system whose origin is fixed at the centre of mass of the drop.

It is assumed, in (13), that the drop is axisymmetric. The unit normal at the drop surface, $\boldsymbol{n}_1$, is defined in terms of F as

$$\boldsymbol{n}_1 \equiv \frac{\nabla F}{|\nabla F|}.$$

The distance between the centre of mass of the drop and the plane of the undisturbed interface, $z = 0$, is denoted as $L(t)$. Since the shape function $f(\hat{\theta}, t)$ is defined relative to local coordinates, fixed at the centre of mass, the right-hand side of (12) is non-zero only if the drop is changing shape. The velocity components $\boldsymbol{n}_1 \cdot \boldsymbol{u}_1$ and $\boldsymbol{n}_1 \cdot \boldsymbol{u}_2$, on the other hand, are defined with respect to a reference frame that is fixed at the plane $z = 0$. Thus, in applying the kinematic condition in terms of $f(\hat{\theta}, t)$, it is necessary to subtract the contribution to $\boldsymbol{u}_1 \cdot \boldsymbol{n}$ that is due to translation of the centre of mass with velocity $-(\partial L/\partial t)\boldsymbol{i}_z$, as shown in (12).

The normal stress component of the stress balance, (11), again contains both a capillary pressure contribution, and a body force contribution. The dimensionless parameters are $Ca_1 \equiv \mu_2 U_\infty/\gamma_{12}$ and $Cg_1 = \mu_2 U_\infty/ga^2(\rho_2-\rho_1)$. However, it should be noted that Cg_1 can be expressed solely in terms of the viscosity ratio, λ_1, due to the definition of U_∞ in (2); namely, $Cg_1 = 2/9\beta$. Thus, the stress balance (11) can be written in the alternative form

$$\boldsymbol{n}_1 \cdot \boldsymbol{T}_2 - \lambda_1 \boldsymbol{n}_1 \cdot \boldsymbol{T}_1 = \frac{1}{Ca_1}(\nabla \cdot \boldsymbol{n}_1)\boldsymbol{n}_1 - \tfrac{9}{2}\beta(-L + f\cos\hat{\theta})\boldsymbol{n}_1 \tag{14}$$

and we see that the problem is completely specified in terms of the five independent parameters Ca_1, Ca_3, Cg_3, λ_1 and λ_3. The coefficient $(-L + f\cos\hat{\theta})$ in the last term is the vertical distance from the reference plane $z = 0$ to a point on the drop surface at the angle $\hat{\theta}$.

It is important to recognize that the equations and boundary conditions (3)–(11) are sufficient to completely determine the drop velocity and pressure fields in all three fluids, as well as the drop shape, the interface shape and the velocity of the centre of mass of the drop. It is tempting to suppose that a macroscopic force balance must be applied in addition to these equations and boundary conditions in order to determine the drop velocity, since this would be true for a solid body. However, a solution of the creeping-flow equations (3)–(5), which satisfies the stress condition (11) or (14), will automatically satisfy the macroscopic balance between the buoyancy forces on the one hand, and the hydrodynamic drag on the other. This fact is demonstrated in the Appendix, where we show that the macro-force balance can be derived directly from (11) and the creeping-motion equations (3)–(5).

3. Solution methodology

Now, we have seen that the problem is to solve (3)–(5), subject to the conditions (6)–(12), to obtain velocity and pressure fields in the three fluids, as well as the drop velocity and shape, and the interface shape, as a function of time. Although the full problem is both nonlinear, and unsteady, owing to the boundary conditions (8), (9), (11), and (12), the governing equations are linear and the problem is ideally suited for solution by the well-known boundary-integral method. We follow earlier studies in our group, cf. Lee & Leal (1982) and Geller *et al.* (1986), and represent the solution in terms of boundary distributions of the single- and double-layer potentials for Stokes' equations, due to Ladyzhenskaya (1963). In this form, we can directly calculate the shape and motion of both the drop and the interface as a function of time, without the necessity of obtaining velocity or pressure fields in the three fluids.

Thus, for an arbitrary point $\boldsymbol{x}$ in any one of the three fluids, we can express the velocity and pressure in the general forms

$$\boldsymbol{u}(\boldsymbol{x}) = \frac{1}{8\pi}\int_S \left[\frac{\boldsymbol{I}}{R}+\frac{(\boldsymbol{x}-\boldsymbol{\eta})(\boldsymbol{x}-\boldsymbol{\eta})}{R^3}\right]\cdot\boldsymbol{T}(\boldsymbol{\eta})\cdot\boldsymbol{n}\,\mathrm{d}S_\eta - \frac{3}{4\pi}\int_S \frac{(\boldsymbol{x}-\boldsymbol{\eta})(\boldsymbol{x}-\boldsymbol{\eta})(\boldsymbol{x}-\boldsymbol{\eta})}{R^5}\cdot\boldsymbol{u}(\boldsymbol{\eta})\cdot\boldsymbol{n}\,\mathrm{d}S_\eta, \tag{15}$$

$$P(\boldsymbol{x}) = \frac{1}{2\pi}\int_S \left[\frac{\boldsymbol{I}}{R^3}-\frac{3(\boldsymbol{x}-\boldsymbol{\eta})(\boldsymbol{x}-\boldsymbol{\eta})}{R^5}\right]\cdot\boldsymbol{u}(\boldsymbol{\eta})\cdot\boldsymbol{n}\,\mathrm{d}S_\eta + \frac{1}{4\pi}\int_S \frac{(\boldsymbol{x}-\boldsymbol{\eta})}{R^3}\cdot\boldsymbol{T}(\boldsymbol{\eta})\cdot\boldsymbol{n}\,\mathrm{d}S_\eta, \tag{16}$$

where S denotes the bounding surface(s) for the fluid in question, η denotes a position on the bounding surface, $\boldsymbol{n}$ is the outer normal to this surface, and $R = |\boldsymbol{x}-\boldsymbol{\eta}|$. In fluid 2, the bounding surface, S, includes both the drop and the interface. Fluid 1 and fluid 3 have one boundary each, the drop surface and the interface, respectively. As is well known, cf. Lee & Leal (1982), the double-layer potentials, i.e. the second terms in (15) and (16), are not continuous, but suffer a jump at the boundaries.

To determine the unknown surface stress or velocity components which act as weighting functions in (15) and (16), we apply the general solutions (15) and (16) *at* the boundaries, and utilize the boundary conditions (7), (8), (10), and (11) to convert them to integral equations. Applying (15) at the boundary of fluid 1, taking account of the jump condition for the double-layer term, we obtain for $\boldsymbol{x}\in S_{\mathrm{D}}$,

$$\tfrac{1}{2}\boldsymbol{u}^{\mathrm{D}}(\boldsymbol{x}) = \frac{1}{8\pi}\int_{S_{\mathrm{D}}}\left[\frac{\boldsymbol{I}}{R}+\frac{\boldsymbol{rr}}{R^3}\right]\cdot\boldsymbol{T}_1^{\mathrm{D}}(\boldsymbol{\eta})\cdot\boldsymbol{n}_1\,\mathrm{d}S_{\mathrm{D}} - \frac{3}{4\pi}\int_{S_{\mathrm{D}}}\frac{\boldsymbol{rrr}}{R^5}\cdot\boldsymbol{u}^{\mathrm{D}}(\boldsymbol{\eta})\cdot\boldsymbol{n}_1\,\mathrm{d}S_{\mathrm{D}}, \tag{17}$$

where $\boldsymbol{r} = \boldsymbol{x} - \boldsymbol{\eta}$ and subscripts and superscripts D indicate that the variables are evaluated at the drop surface. The stress tensor, $\boldsymbol{T}_1^{\mathrm{D}}$, is evaluated as the drop surface is approached from fluid 1. Similarly, applying (15) to the body of fluid 2, we obtain for $\boldsymbol{x} \in S_{\mathrm{D}}$,

$$\tfrac{1}{2}\boldsymbol{u}^{\mathrm{D}}(\boldsymbol{x}) = -\frac{1}{8\pi}\int_{S_{\mathrm{D}}}\left[\frac{\boldsymbol{I}}{R}+\frac{\boldsymbol{rr}}{R^3}\right]\cdot\boldsymbol{T}_2^{\mathrm{D}}(\boldsymbol{\eta})\cdot\boldsymbol{n}_1\,\mathrm{d}S_{\mathrm{D}} - \frac{1}{8\pi}\int_{S_{\mathrm{I}}}\left[\frac{\boldsymbol{I}}{R}+\frac{\boldsymbol{rr}}{R^3}\right]\cdot\boldsymbol{T}_2^{\mathrm{I}}(\boldsymbol{\eta})\cdot\boldsymbol{n}_3\,\mathrm{d}S_{\mathrm{I}}$$
$$+\frac{3}{4\pi}\int_{S_{\mathrm{D}}}\left[\frac{\boldsymbol{rrr}}{R^5}\right]\cdot\boldsymbol{u}^{\mathrm{D}}(\boldsymbol{\eta})\cdot\boldsymbol{n}_1\,\mathrm{d}S_{\mathrm{D}} + \frac{3}{4\pi}\int_{S_{\mathrm{I}}}\left[\frac{\boldsymbol{rrr}}{R^5}\right]\cdot\boldsymbol{u}^{\mathrm{I}}\cdot\boldsymbol{n}_3\,\mathrm{d}S_{\mathrm{I}}; \quad (18)$$

and for $\boldsymbol{x} \in S_{\mathrm{I}}$,

$$\tfrac{1}{2}\boldsymbol{u}^{\mathrm{I}}(\boldsymbol{x}) = -\frac{1}{8\pi}\int_{S_{\mathrm{D}}}\left[\frac{\boldsymbol{I}}{R}+\frac{\boldsymbol{rr}}{R^3}\right]\cdot\boldsymbol{T}_2^{\mathrm{D}}(\boldsymbol{\eta})\cdot\boldsymbol{n}_1\,\mathrm{d}S_{\mathrm{D}} - \frac{1}{8\pi}\int_{S_{\mathrm{I}}}\left[\frac{\boldsymbol{I}}{R}+\frac{\boldsymbol{rr}}{R^3}\right]\cdot\boldsymbol{T}_2^{\mathrm{I}}(\boldsymbol{\eta})\cdot\boldsymbol{n}_3\,\mathrm{d}S_{\mathrm{I}}$$
$$+\frac{3}{4\pi}\int_{S_{\mathrm{D}}}\left[\frac{\boldsymbol{rrr}}{R^5}\right]\cdot\boldsymbol{u}^{\mathrm{D}}(\boldsymbol{\eta})\cdot\boldsymbol{n}_1\,\mathrm{d}S_{\mathrm{D}} + \frac{3}{4\pi}\int_{S_{\mathrm{I}}}\left[\frac{\boldsymbol{rrr}}{R^5}\right]\cdot\boldsymbol{u}^{\mathrm{I}}(\boldsymbol{\eta})\cdot\boldsymbol{n}_3\,\mathrm{d}S_{\mathrm{I}}. \quad (19)$$

Here, subscripts and superscripts I indicate quantities evaluated at the bulk interface. Again, $\boldsymbol{T}_2^{\mathrm{D}}$ and $\boldsymbol{T}_2^{\mathrm{I}}$ are evaluated as the drop surface or the interface is approached from fluid 2. Finally, applying (15) to the body of fluid 3, we obtain for $\boldsymbol{x} \in S_{\mathrm{I}}$,

$$\tfrac{1}{2}\boldsymbol{u}^{\mathrm{I}}(\boldsymbol{x}) = \frac{1}{8\pi}\int_{S_{\mathrm{I}}}\left[\frac{\boldsymbol{I}}{R}+\frac{\boldsymbol{rr}}{R}\right]\cdot\boldsymbol{T}_3^{\mathrm{I}}(\boldsymbol{\eta})\cdot\boldsymbol{n}_3\,\mathrm{d}S - \frac{3}{4\pi}\int_{S_{\mathrm{I}}}\left[\frac{\boldsymbol{rrr}}{R^5}\right]\cdot\boldsymbol{u}^{\mathrm{I}}(\boldsymbol{\eta})\cdot\boldsymbol{n}_3\,\mathrm{d}S, \quad (20)$$

where $\boldsymbol{T}_3^{\mathrm{I}}$ is the stress tensor evaluated as the interface is approached from fluid 3.

The stress at the drop surface, $\boldsymbol{T}_1^{\mathrm{D}}$, can be eliminated from (17) and (18) using the boundary condition (11). To do this, we add (17) and (18) together to give

$$\tfrac{1}{2}(\lambda_1+1)\,\boldsymbol{u}^{\mathrm{D}}(\boldsymbol{x}) = -\frac{1}{8\pi}\int_{S_{\mathrm{D}}}\left[\frac{\boldsymbol{I}}{R}+\frac{\boldsymbol{rr}}{R^3}\right]\cdot\boldsymbol{Q}^{\mathrm{D}}(f)\,\mathrm{d}S_{\mathrm{D}} - \frac{1}{8\pi}\int_{S_{\mathrm{I}}}\left[\frac{\boldsymbol{I}}{R}+\frac{\boldsymbol{rr}}{R^3}\right]\cdot\boldsymbol{T}_2^{\mathrm{I}}(\boldsymbol{\eta})\cdot\boldsymbol{n}_3\,\mathrm{d}S_{\mathrm{I}}$$
$$+\frac{3}{4\pi}(1-\lambda_1)\int_{S_{\mathrm{D}}}\left[\frac{\boldsymbol{rrr}}{R^5}\right]\cdot\boldsymbol{u}^{\mathrm{D}}(\boldsymbol{\eta})\cdot\boldsymbol{n}_1\,\mathrm{d}S_{\mathrm{D}} + \frac{3}{4\pi}\int_{S_{\mathrm{I}}}\frac{\boldsymbol{rrr}}{R^5}\cdot\boldsymbol{u}^{\mathrm{I}}(\boldsymbol{\eta})\cdot\boldsymbol{n}_3\,\mathrm{d}S_{\mathrm{I}}. \quad (21)$$

Here, the function $\boldsymbol{Q}^{\mathrm{D}}(f)$ is the stress difference at the drop surface

$$\boldsymbol{Q}^{\mathrm{D}}(f) \equiv \boldsymbol{n}\cdot\boldsymbol{T}_2 - \lambda_1\boldsymbol{n}\cdot\boldsymbol{T}_1 = \boldsymbol{n}_1\frac{1}{Ca_1}\left\{\frac{K_{\mathrm{D}}}{f}(3-K_{\mathrm{D}}^2) - \frac{K_{\mathrm{D}}}{f^2}\left[\frac{\cos\hat{\theta}}{\sin\hat{\theta}}\left(\frac{\partial f}{\partial\hat{\theta}}\right)\right.\right.$$
$$\left.\left.+K_{\mathrm{D}}^2\left(\frac{\partial^2 f}{\partial\hat{\theta}^2}\right)\right]\right\} - \tfrac{2}{3}\beta(-L+f\cos\hat{\theta})\,\boldsymbol{n}_1, \quad (22)$$

with

$$K_{\mathrm{D}} = \frac{1}{[1+f^{-2}(\partial f/\partial\hat{\theta})^2]^{\frac{1}{2}}}.$$

Similarly, (19) and (20) can be added together to eliminate $\boldsymbol{T}_3^{\mathrm{D}}$, using the boundary condition (8):

$$\tfrac{1}{2}(\lambda_3+1)\,\boldsymbol{u}^{\mathrm{I}}(\boldsymbol{x}) = -\frac{1}{8\pi}\int_{S_{\mathrm{D}}}\left[\frac{\boldsymbol{I}}{R}+\frac{\boldsymbol{rr}}{R^3}\right]\cdot\boldsymbol{T}_2^{\mathrm{D}}(\boldsymbol{\eta})\cdot\boldsymbol{n}_1\,\mathrm{d}S_{\mathrm{D}} - \frac{1}{8\pi}\int_{S_{\mathrm{I}}}\left[\frac{\boldsymbol{I}}{R}+\frac{\boldsymbol{rr}}{R^3}\right]\cdot\boldsymbol{Q}^{\mathrm{I}}(h)\,\mathrm{d}S_{\mathrm{I}}$$
$$+\frac{3}{4\pi}\int_{S_{\mathrm{D}}}\left[\frac{\boldsymbol{rrr}}{R^5}\right]\cdot\boldsymbol{u}^{\mathrm{D}}(\boldsymbol{\eta})\cdot\boldsymbol{n}_1\,\mathrm{d}S_{\mathrm{D}} + \frac{3}{4\pi}(1-\lambda_3)\int_{S_{\mathrm{I}}}\left[\frac{\boldsymbol{rrr}}{R^5}\right]\cdot\boldsymbol{u}^{\mathrm{I}}(\boldsymbol{\eta})\cdot\boldsymbol{n}_3\,\mathrm{d}S_{\mathrm{I}}, \quad (23)$$

where $\boldsymbol{Q}^{\mathrm{I}}(h)$ is the stress difference at the interface

$$\boldsymbol{Q}^{\mathrm{I}}(h) = \boldsymbol{n}\cdot\boldsymbol{T}_2 - \lambda_3 \boldsymbol{n}\cdot\boldsymbol{T}_3 = \boldsymbol{n}_3 \frac{1}{Ca_3}\left[\frac{K_{\mathrm{I}}}{r}\left(\frac{\partial h}{\partial r}\right) + K_{\mathrm{I}}^3\left(\frac{\partial^2 h}{\partial r^2}\right)\right] - \frac{1}{Cg_3} h\boldsymbol{n}_3 \tag{24}$$

with

$$K_{\mathrm{I}} = \frac{1}{[1+(\partial h/\partial r)^2]^{\frac{1}{2}}}.$$

Equations (18), (19), (21), and (23) are a self-contained set from which the unknown components of $\boldsymbol{u}^{\mathrm{D}}$, $\boldsymbol{u}^{\mathrm{I}}$, $\boldsymbol{T}_2^{\mathrm{D}}$ and $\boldsymbol{T}_2^{\mathrm{I}}$ can be determined at some instant if the geometry of the problem – i.e. the drop position and shape and the interface shape – is specified at that instant. The resulting solutions satisfy all of the equations and boundary conditions of the problem except for the kinematic conditions (9) and (12). However, with $\boldsymbol{u}^{\mathrm{I}}$ and $\boldsymbol{u}^{\mathrm{D}}$ known from the solution at time t, these conditions can be used to increment the locations of the drop surface and the interface to a time increment, Δt, later, thus determining a new shape and position for the drop and a new shape for the interface, and the process repeated.

The kinematic condition (9) is applied in the approximate form

$$h_{j+1} = h_j + [\boldsymbol{u}_j^{\mathrm{I}}\cdot\boldsymbol{n}_{3j}]\,\Delta t \frac{1}{K_{\mathrm{I}j}}, \tag{25}$$

where the subscript j denotes quantities that are known at the jth time step. (Later, more advanced versions of the numerical algorithm described here use implicit time-stepping schemes which allow larger time steps and increased stability.)

The kinematic condition (12), at the top surface, is a little trickier to apply. The problem is that the normal velocity component $\boldsymbol{u}^{\mathrm{D}}\cdot\boldsymbol{n}_1$ contains a contribution due both to the change in shape, and to the translation of the centre of mass, i.e.

$$\boldsymbol{n}_1\cdot\boldsymbol{u}^{\mathrm{D}} = -\frac{\partial L}{\partial t}(\boldsymbol{n}_1\cdot\boldsymbol{i}_z) + \frac{1}{|\nabla F|}\frac{\partial f}{\partial t}, \tag{26}$$

and these conditions must be separated. To do this, we must apply (26) subject to the condition that the centre of mass of the drop remain coincident with the origin of the 'local' spherical coordinate system that is used to define f, i.e. that the centre of mass in this system be fixed at the origin. In view of the assumed axisymmetry of the drop, this requires

$$0 = \int \hat{z}\,\mathrm{d}V_{\mathrm{D}}, \tag{27}$$

where $\hat{z} = \hat{r}_s\cos\hat{\theta}$. When (27) is expressed in terms of the local spherical coordinate system, and integrated in the aximuthal direction, we obtain

$$0 = 2\pi\int_{\hat{\theta}=0}^{\pi}\int_{\hat{r}_{\mathrm{s}}=0}^{f} \hat{r}_{\mathrm{s}}^3\cos\hat{\theta}\sin\hat{\theta}\,\mathrm{d}\hat{\theta}\,\mathrm{d}\hat{r}_{\mathrm{s}}. \tag{28}$$

Integrating once more with respect to $\hat{r}_{\mathrm{s}}$, and letting $\hat{\eta} = \cos\hat{\theta}$, we find

$$\int_{\hat{\eta}=-1}^{1} f^4\hat{\eta}\,\mathrm{d}\hat{\eta} = 0. \tag{29}$$

Hence, the kinematic condition (26) is applied in the approximate form

$$f_{j+1} = f_j + \frac{1}{K_{\mathrm{D}j}}\left[\left(\boldsymbol{u}_j^{\mathrm{D}} + \frac{L_{j+1}-L_j}{\Delta t}\boldsymbol{i}_z\right)\cdot\boldsymbol{n}_{1j}\right]\Delta t \tag{30}$$

subject to the constraint (29), which can be expressed in the form

$$\int_{\hat{\eta}=-1}^{1} [f_j + \Delta f_j]^4 \,\hat{\eta}\,\mathrm{d}\hat{\eta} = 0, \tag{31}$$

where

$$\Delta f_j \equiv \frac{1}{K_{\mathrm{D}j}}\left[\boldsymbol{u}_j^{\mathrm{D}} + \frac{L_{j+1}-L_j}{\Delta t}\boldsymbol{i}_{\hat{z}}\right]\cdot \boldsymbol{n}_{1j}\,\Delta t.$$

The position of the centre of mass at time step $j+1$ is obtained from (31). With L_{j+1} known, the kinematic condition (30) then yields the shape function at $j+1$, i.e. f_{j+1}.

A final condition on changes in the drop shape is that the volume should remain constant. In principal, this condition is satisfied automatically by solutions of the boundary-integral equations; however, there is a well-known difficulty with spurious eigensolutions in the limit $\lambda_1 \to 0$ (cf. Youngren & Acrivos 1976), and one needs to be concerned with the accumulative buildup of errors, which may be very small at each time step. The constant-volume condition can be written in the form

$$\int_0^{\pi} f^3 \sin\theta\,\mathrm{d}\theta = 2, \tag{32}$$

and this condition was checked at each time step during the present calculations. The maximum volume change over the complete calculated trajectory was always less than 2% for the cases that are presented below.

Since the drop is assumed to approach the interface symmetrically, the surface integrals in (18), (19), (21), and (23) can be reduced to line integrals by analytically integrating in the azimuthal direction. Thus, for axisymmetric flows, (18), (19), (21), and (23) become

$$\frac{1}{2}\begin{pmatrix} u_r^{\mathrm{D}}(\boldsymbol{x}) \\ u_z^{\mathrm{D}}(\boldsymbol{x}) \end{pmatrix} = -\frac{1}{8\pi}\int_{S_{\mathrm{D}}} \boldsymbol{B}(\boldsymbol{x},\boldsymbol{\eta})\cdot\begin{pmatrix} T_{nr}^{\mathrm{D}} \\ T_{nz}^{\mathrm{D}} \end{pmatrix}\mathrm{d}l_{\mathrm{D}} - \frac{1}{8\pi}\int_{S_{\mathrm{I}}} \boldsymbol{B}(\boldsymbol{x},\boldsymbol{\eta})\cdot\begin{pmatrix} T_{nr}^{\mathrm{I}} \\ T_{nz}^{\mathrm{I}} \end{pmatrix}\mathrm{d}l_{\mathrm{I}}$$
$$+\frac{3}{4\pi}\int_{S_{\mathrm{D}}} \boldsymbol{C}(\boldsymbol{x},\boldsymbol{\eta})\cdot\begin{pmatrix} u_r^{\mathrm{D}} \\ u_z^{\mathrm{D}} \end{pmatrix}\mathrm{d}l_{\mathrm{D}} + \frac{3}{4\pi}\int_{S_{\mathrm{I}}} \boldsymbol{C}(\boldsymbol{x},\boldsymbol{\eta})\cdot\begin{pmatrix} u_r^{\mathrm{I}} \\ u_z^{\mathrm{I}} \end{pmatrix}\mathrm{d}l_{\mathrm{I}}, \tag{33}$$

$$\frac{1}{2}\begin{pmatrix} u_r^{\mathrm{I}}(\boldsymbol{x}) \\ u_z^{\mathrm{I}}(\boldsymbol{x}) \end{pmatrix} = -\frac{1}{8\pi}\int_{S_{\mathrm{D}}} \boldsymbol{B}(\boldsymbol{x},\boldsymbol{\eta})\cdot\begin{pmatrix} T_{nr}^{\mathrm{D}} \\ T_{nz}^{\mathrm{D}} \end{pmatrix}\mathrm{d}l_{\mathrm{D}} - \frac{1}{8\pi}\int_{S_{\mathrm{I}}} \boldsymbol{B}(\boldsymbol{x},\boldsymbol{\eta})\cdot\begin{pmatrix} T_{nr}^{\mathrm{I}} \\ T_{nz}^{\mathrm{I}} \end{pmatrix}\mathrm{d}l_{\mathrm{I}}$$
$$+\frac{3}{4\pi}\int_{S_{\mathrm{D}}} \boldsymbol{C}(\boldsymbol{x},\boldsymbol{\eta})\cdot\begin{pmatrix} u_r^{\mathrm{D}} \\ u_z^{\mathrm{D}} \end{pmatrix}\mathrm{d}l_{\mathrm{D}} + \frac{3}{4\pi}\int_{S_{\mathrm{I}}} \boldsymbol{C}(\boldsymbol{x},\boldsymbol{\eta})\cdot\begin{pmatrix} u_r^{\mathrm{I}} \\ u_z^{\mathrm{I}} \end{pmatrix}\mathrm{d}l_{\mathrm{I}}, \tag{34}$$

$$\tfrac{1}{2}(\lambda_1+1)\begin{pmatrix} u_r^{\mathrm{D}}(\boldsymbol{x}) \\ u_z^{\mathrm{D}}(\boldsymbol{x}) \end{pmatrix} = -\frac{1}{8\pi}\int_{S_{\mathrm{D}}} \boldsymbol{B}(\boldsymbol{x},\boldsymbol{\eta})\cdot\begin{pmatrix} Q_r^{\mathrm{D}}(f) \\ Q_z^{\mathrm{D}}(f) \end{pmatrix}\mathrm{d}l_{\mathrm{D}} - \frac{1}{8\pi}\int_{S_{\mathrm{I}}} \boldsymbol{B}(\boldsymbol{x},\boldsymbol{\eta})\cdot\begin{pmatrix} T_{nr}^{\mathrm{I}} \\ T_{nz}^{\mathrm{I}} \end{pmatrix}\mathrm{d}l_{\mathrm{I}}$$
$$+\frac{3}{4\pi}(1-\lambda_1)\int_{S_{\mathrm{D}}} \boldsymbol{C}(\boldsymbol{x},\boldsymbol{\eta})\cdot\begin{pmatrix} u_r^{\mathrm{D}} \\ u_z^{\mathrm{D}} \end{pmatrix}\mathrm{d}l_{\mathrm{D}} + \frac{3}{4\pi}\int_{S_{\mathrm{I}}} \boldsymbol{C}(\boldsymbol{x},\boldsymbol{\eta})\cdot\begin{pmatrix} u_r^{\mathrm{I}} \\ u_z^{\mathrm{I}} \end{pmatrix}\mathrm{d}l_{\mathrm{I}}, \tag{35}$$

$$\tfrac{1}{2}(\lambda_3+1)\begin{pmatrix} u_r^{\mathrm{I}}(\boldsymbol{x}) \\ u_z^{\mathrm{I}}(\boldsymbol{x}) \end{pmatrix} = -\frac{1}{8\pi}\int_{S_{\mathrm{D}}} \boldsymbol{B}(\boldsymbol{x},\boldsymbol{\eta})\cdot\begin{pmatrix} T_{nr}^{\mathrm{D}} \\ T_{nz}^{\mathrm{D}} \end{pmatrix}\mathrm{d}l_{\mathrm{D}} - \frac{1}{8\pi}\int_{S_{\mathrm{I}}} \boldsymbol{B}(\boldsymbol{x},\boldsymbol{\eta})\cdot\begin{pmatrix} Q_r^{\mathrm{I}}(h) \\ Q_z^{\mathrm{I}}(h) \end{pmatrix}\mathrm{d}l_{\mathrm{I}}$$
$$+\frac{3}{4\pi}\int_{S_{\mathrm{D}}} \boldsymbol{C}(\boldsymbol{x},\boldsymbol{\eta})\cdot\begin{pmatrix} u_r^{\mathrm{D}} \\ u_z^{\mathrm{D}} \end{pmatrix}\mathrm{d}l_{\mathrm{D}} + \frac{3}{4\pi}(1-\lambda_3)\int_{S_{\mathrm{I}}} \boldsymbol{C}(\boldsymbol{x},\boldsymbol{\eta})\cdot\begin{pmatrix} u_r^{\mathrm{I}} \\ u_z^{\mathrm{I}} \end{pmatrix}\mathrm{d}l_{\mathrm{I}}, \tag{36}$$

where

$$\mathrm{d}l_{\mathrm{D}} = f\sin\hat{\theta}\left[f^2 + \left(\frac{\partial f}{\partial\hat{\theta}}\right)^2\right]^{\frac{1}{2}}\mathrm{d}\theta$$

and $$\mathrm{d}l_{\mathrm{I}} = r\left[1+\left(\frac{\partial h}{\partial r}\right)^2\right]^{\frac{1}{2}}\mathrm{d}r.$$

The quantities $\boldsymbol{B}$ and $\boldsymbol{C}$ are tensors whose elements consist of elliptic integrals

$$\boldsymbol{B}(\boldsymbol{x},\boldsymbol{\eta}) = \begin{bmatrix} B_{rr} & B_{rz} \\ B_{zr} & B_{zz} \end{bmatrix}, \quad \boldsymbol{C}(\boldsymbol{x},\boldsymbol{\eta}) = \begin{bmatrix} C_{rr} & C_{rz} \\ C_{zr} & C_{zz} \end{bmatrix}. \tag{37}$$

The elements of $\boldsymbol{B}$ and $\boldsymbol{C}$ are given by Lee & Leal (1982).

There are eight linear integral equations (33)–(36) for eight unknown functions, u_r^{D}, u_z^{D}, u_r^{I}, u_z^{I}, T_{nr}^{D}, T_{nz}^{D}, T_{nr}^{I}, and T_{nz}^{I}. As in the works of Lee & Leal (1982) and Geller *et al.* (1986), a collocation method was used to approximate the linear integral equations by a system of linear algebraic equations. To apply the collocation technique, the drop surface and the interface were divided into small elements so that $\boldsymbol{u}^{\mathrm{D}}, \boldsymbol{u}^{\mathrm{I}}, \boldsymbol{T}_2^{\mathrm{D}}, \boldsymbol{T}_2^{\mathrm{I}}$ could be approximated as constants within each element (equal to the values at the centre of the element). Thus, we obtain a system of $(4N_{\mathrm{D}}+4N_{\mathrm{I}})$ linear algebraic equations where N_{D} and N_{I} are the number of elements on the drop surface and the interface respectively. The integrals in (33)–(36) were evaluated by Gauss quadrature, and the system of linear equations was solved by Gaussian elimination. When $\boldsymbol{x}\rightarrow\boldsymbol{\eta}$, the integrals in (18), (19), (21), and (23) develop an integrable singularity. Hence, the integrals must be evaluated analytically over a small neighbourhood of $\boldsymbol{x}$ and this is done using a linear expansion of the integrands (cf. Lee & Leal 1982; Geller *et al.* 1986). Finally, we note that the interface shape functions were approximated using a cubic spline fit through the centre of the surface elements, with continuity of the function and its first and second derivatives imposed at the end points of each segment.

4. Results

In the present study, we consider the case when fluids 1 and 3 are identical. For this case, $Ca_1 = Ca_3 = Ca$, $\lambda_1 = \lambda_3 = \lambda$, and $Cg_3 = Cg_1 = 2/9\beta$. This is the system occurring most frequently in industrial processes (e.g. liquid–liquid extraction). When fluid 1 is the same as fluid 3, a slight adaptation of the macroscopic force balance used by Geller *et al.* (1986) for a solid sphere approaching an interface shows that coalescence must occur via a film-drainage configuration (because the density of fluid 1 is the same as the density of fluid 3), though this is not true in general.

Of course, the drop shape and interface configuration at any instant depend on the initial configuration. In the present calculations, we always initiate our solution with a spherical drop and a flat interface, as is appropriate for a drop that is released from a predetermined position into a quiescent fluid system. At the end of this paper, we briefly consider the influence of various starting positions on the evolution of drop and interface shapes. In this first part, however, the calculations were all initiated with $L_{t=0} = 3$. We shall see later that this starting distance is sufficient to provide a good approximation of drop and interface shapes for the 'ideal' case, $L_{t=0} = \infty$, where the steady drop shape is actually spherical and the interface is undisturbed.

When the collocation method, described in the preceeding section, is applied to the integral equations (33)–(36), the domain of the interface must be truncated at some large, but finite distance from the central symmetry axis. It was shown by Lee & Leal (1982) that the integrals decay like $1/r^2$ for large r for the case of a solid sphere approaching an interface. In figure 2, $-\boldsymbol{u}^{\mathrm{I}}\cdot\boldsymbol{n}_3$ on the interface is plotted for the present problem as a function of r for two cases, $Ca = 10, \lambda = 0.1$ and $Ca = 10$,

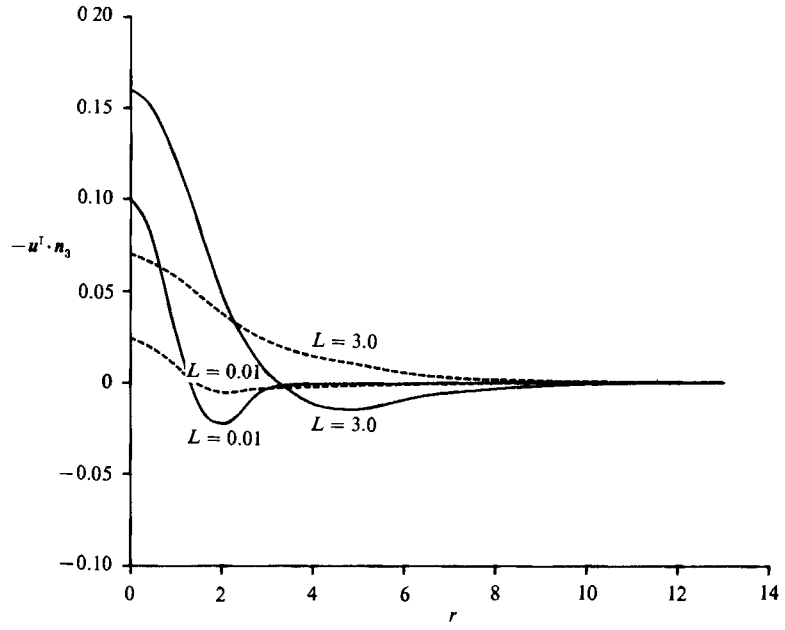

FIGURE 2. Dimensionless normal velocity on the interface, $-\boldsymbol{u}^{I}\cdot\boldsymbol{n}_3$, as a function of the dimensionless radial distance, r; ——, $Ca = 10, \lambda = 0.1$; – – – –, $Ca = 10, \lambda = 10$.

$\lambda = 10$, when the domain of the interface is truncated at $r = 13$. It can be seen that $\boldsymbol{u}^{I}\cdot\boldsymbol{n}_3$ becomes almost zero beyond $r \sim 10$ for both $L = 0.01$ and 3. In the calculations reported later, the interface was usually truncated at $r = 13$.

In this numerical study, the drop surface and interface were discretized into small elements in which $\boldsymbol{u}^{D}, \boldsymbol{T}_2^{D}, \boldsymbol{u}^{I}, \boldsymbol{T}_2^{I}$ are constant. Non-uniform elements were used on the drop. For the initially spherical drop, uniform elements were used but more elements were added to the region where $\boldsymbol{u}^{D}, \boldsymbol{T}_2^{D}$ varied rapidly as the drop approached the interface. Usually 20 elements were used for a spherical drop, and up to 30 elements were used as the drop deformed. On the interface, the region close to the drop was discretized with smaller elements, and increasingly larger elements were used for larger values of $\boldsymbol{r}$.

Time enters the problem only through the kinematic conditions (9) and (12), whose treatment in the solution scheme was discussed in the preceding section. Typically, in the calculations reported below, time increments Δt varied from 0.02 to 0.06. For the initially spherical drop at $L_{t=0} = 3$, the value $\Delta t = 0.06$ was adequate. However, as the drop approached the interface, shorter time steps were necessary. When a shorter time step was introduced, calculations were repeated using the shorter time step for a moderate overlap region with the old larger time step. If the difference in the shapes was greater than 2%, then the overlap region was increased until the difference was 2% or less. Eventually, the continual decrease in Δt, and the rapidly decreasing rate of droplet or interface motion, caused us to reach a point of sufficiently diminished return that the calculations were stopped. Generally speaking, this occurred when the minimum film thickness in the region between the drop and the interface was less than 20% of the undeformed drop radius. In fact, the final film thickness was usually considerably smaller than this, and only decreasing extremely slowly when the calculations were terminated. Nevertheless, these 'films' are still somewhat thicker

than the intended regime of the 'film-drainage' models (cf. Lin & Slattery 1982), and this makes direct comparison with these theories difficult. We view the present results as complementary to those obtained via film-drainage calculations, and likely to be indicative of the qualitative connection between 'initial' film geometry and the independent dimensionless parameters λ and Ca. Of course, the film geometry, in the present case, is completely determined by the prior history of motion and the initial configuration. In addition, we consider the complete drop and interface shapes and allow for fluid motion in all parts of the domain.

4.1. *The effects of λ and Ca*

Calculations were carried out for cases when $\lambda = 0.1, 1, 10$ and $Ca = 0.2, 1, 10$. The initial position of the drop is 3 radii away from the interface. Resulting shapes as the drop approaches the interface are shown in figures 3, 4, and 5. The film thickness at the symmetry line, H_{cen}, and the minimum film thickness, H_{min}, are plotted against time, t, in figure 6. In figure 7, drop velocities are plotted against L as the drop approaches the interface. In figures 4 and 5, the drop and interface shapes are drawn for three distances, L, relative to the interface, $L = 1.0, 0.5, 0.01$ when $Ca = 1.0$ and 10. In figure 3, when $Ca = 0.2$, the dotted lines represent $L = 0.36, 0.29, 0.28$ for $\lambda = 0.1, 1, 10$ respectively because $L = 0.01$ cannot be reached by the drop in this case.

The change most obvious in figures 3–5 is the increasing degree of deformation for larger values of Ca at a particular fixed value of λ, and the qualitative shift in the mode of deformation from drops which are flattened in the front and relatively undeformed at the back for $Ca = 0.2$, to shapes which are flattened (and even indented) at the back and relatively undeformed at the front for $Ca = 10$. The mechanism for the first mode of deformation seems relatively obvious, at least qualitatively. However, the mechanism for indentation at the back in this zero-Reynolds-number flow is not clear to us at this time.

Although the changes in drop shape with Ca are amusing, the dependence of drop shape on the viscosity ratio for fixed Ca is of more interest in the context of previous studies of film-drainage geometries. In particular, for each of the three values of Ca studied, careful examination of figures 3–5 reveals three quite distinct types of film geometry (and thus, presumably, three distinct modes of film drainage, though one must be somewhat cautious on this owing to the relatively thick films produced). In the first type, which appears for all three Ca values at $\lambda = 0.1$, the film between the drop and the interface is thinnest at $r = 0$, and the film thickness increases monotonically as r increases. This type of film profile is often associated with 'rapid drainage' and occurs in the present case for systems with low λ, for which the drop does approach the interface faster than for high-λ systems. For $\lambda = 1.0$, the variation of the film thickness with r is so slight that the film appears to be almost uniform in thickness up to some radius, and the film drains almost uniformly as the drop moves closer to the interface. For instance, the film has uniform thickness between $0 \leqslant r \leqslant 0.7$ for $Ca = 0.2$. Finally, for $\lambda = 10$, dimpled drainage occurs in which the film is thinnest at a rim of finite radius, rather than at the centre $r = 0$. For example, for $Ca = 0.2$, the film is thinnest at $r \approx 0.66$. This is also shown in figure 6 where the dotted line for H_{min} diverges from the solid line for H_{cen} at $t = 7.72$. When the minimum thickness occurs at the rim, experimental studies of Charles & Mason (1960), Hodgson & Woods (1969), and Burrill & Woods (1973) show that rupture normally occurs off-centre as a consequence of an apparent physico–chemical instability.

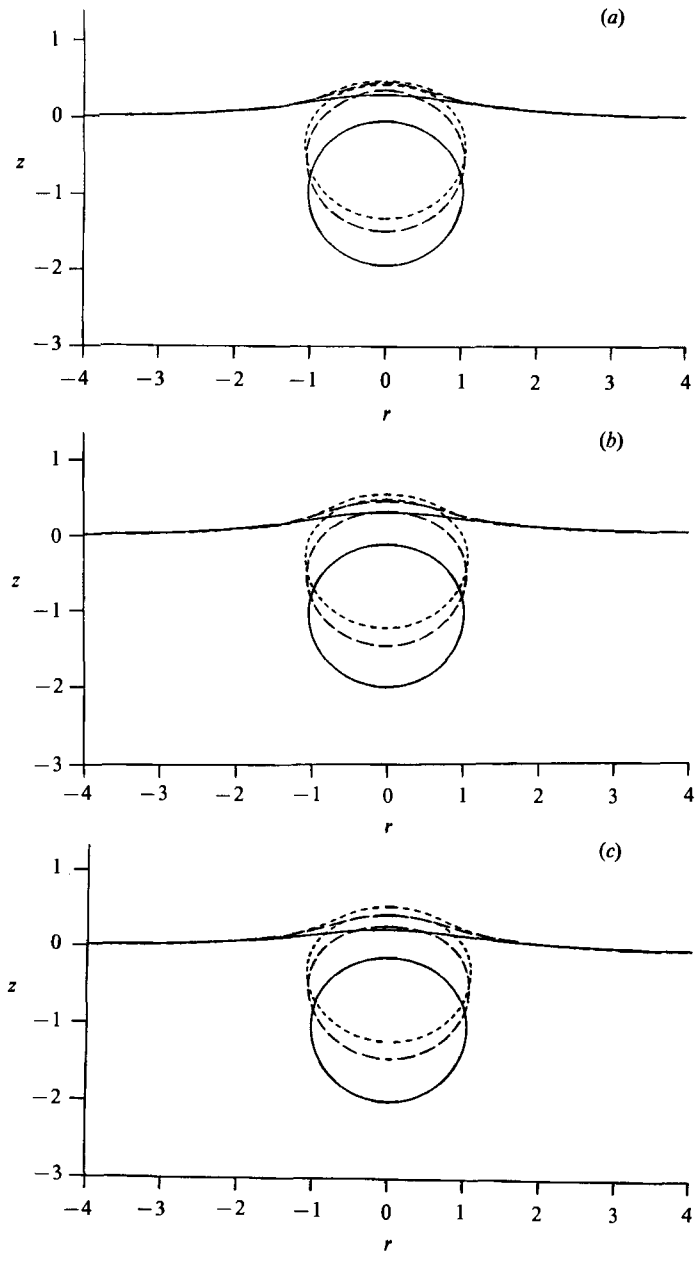

FIGURE 3. Shapes of the drop and the interface for $Ca = 0.2$ and (*a*) $\lambda = 0.1$, (*b*) 1.0, (*c*) 10; ——, $L = 1.0$ (all λ); – – – –, $L = 0.5$ (all λ); - - - -, $L = 0.36, 0.29, 0.28$ (for $\lambda = 0.1, 1.0, 10$ respectively).

All three modes of film drainage described above have been observed experimentally by Hodgson & Woods (1969) and Burrill & Woods (1973) for fluid systems with surfactants. However, these authors attributed the different modes to different levels of mobility of the interface(s). Film-drainage theories with complete slip (zero tangential shear stress) applied at the boundaries predict drainage with the minimum film thickness at the symmetry axis, while film-drainage theories with no-

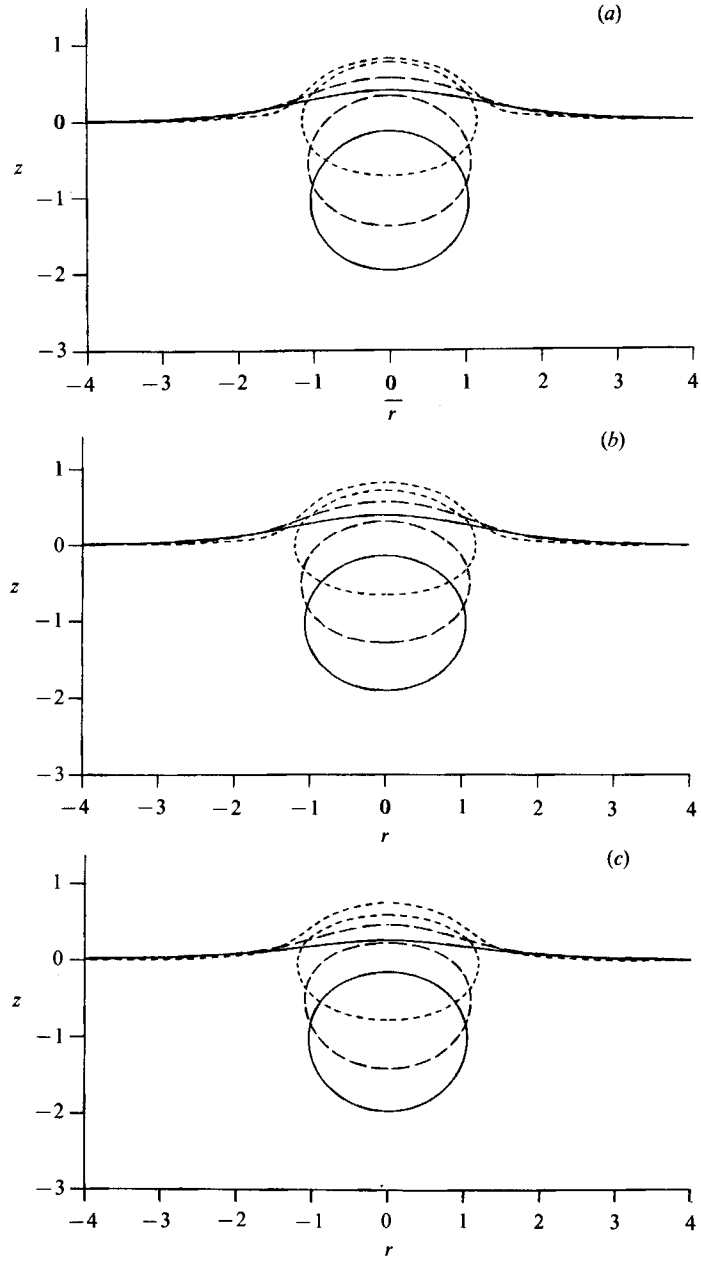

FIGURE 4. Shapes of the drop and the interface for $Ca = 1$ and (*a*) $\lambda = 0.1$, (*b*) 1.0, (*c*) 10; ——, $L = 1.0$; – – – –, $L = 0.5$; - - - -, $L = 0.01$.

slip conditions at the film boundaries yield a film configuration with the point of minimum thickness on a ring away from the symmetry axis. This is not inconsistent with the experimental observations for surfactant systems cited above, but the present results show that high-viscosity fluids in the drop and its bulk homophase can also lead to the dimpled film configuration. Indeed, comparison with the calculations of Geller *et al.* (1986) for a solid sphere approaching an interface shows

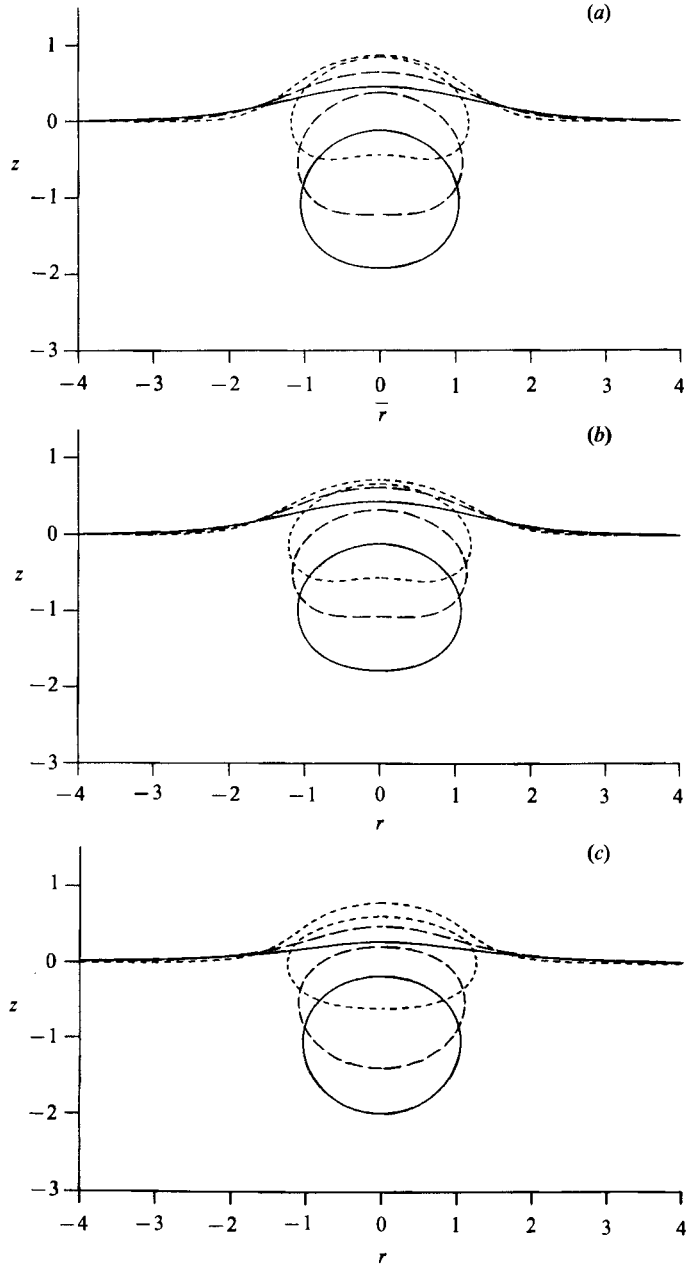

FIGURE 5. Shapes of the drop and the interface for $Ca = 10$ and (*a*) $\lambda = 0.1$, (*b*) 1.0, (*c*) 10; ——, $L = 1.0$; – – – –, $L = 0.5$; - - - -, $L = 0.01$.

that a 'dimpled film' configuration also occurs in that case even when the fluid across the interface has a *low* viscosity, cf. the resuts for $\lambda = 0.022, Ca = 0.464, Cg = 0.089$ (figures 16 and 17 of Geller *et al.*) which can be compared with the present results for $\lambda = 0.1, Ca = 0.2$ (and $Cg = 2/9\beta = 0.32$) where we obtained a minimum film thickness at the symmetry axis. Thus, apparently, immobilization of even one side of the film is sufficient to produce a transition from the 'rapid' drainage mode to the 'dimpled' drainage configuration.

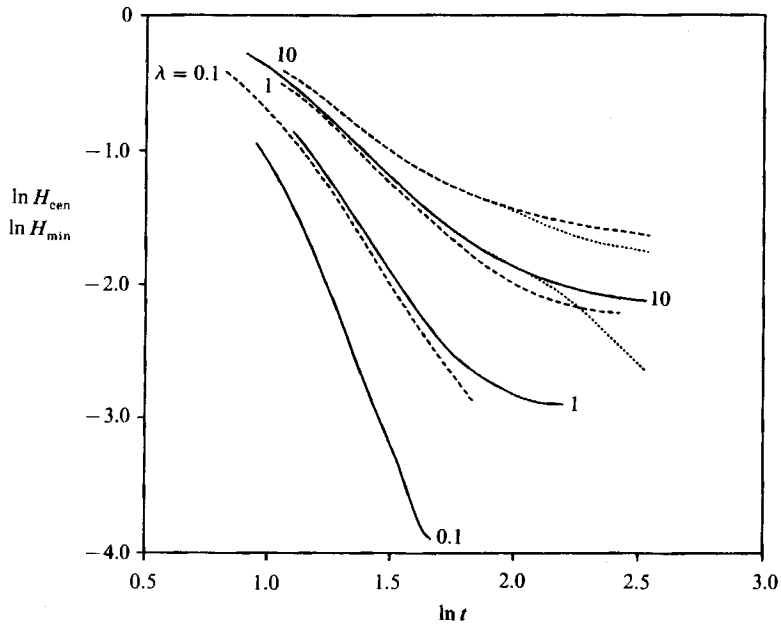

FIGURE 6. Dimensionless film thickness at the centreline, H_{cen}, and at the rim, H_{min}, as a function of the dimensionless time. ——, $\ln H_{cen}$ for $Ca = 0.2$; – – – –, $\ln H_{cen}$ for $Ca = 10$; · · · · ·, $\ln H_{min}$.

The main practical significance of the 'dimpled' configuration is that film drainage occurs more slowly than when the thinnest part of the film is at the symmetry axis, and thus, all else being equal, the coalescence process is inhibited. This is illustrated in figure 6, which shows that the rate of film thinning for $\lambda = 10$ is always smaller than for $\lambda = 0.1$ or 1. This is primarily a consequence of the differences in film geometry. (The timescale inherent in figure 6 includes the difference in characteristic velocity of the drop for the different values of λ.) It will be noted that the results in figure 6 have been presented in the form of a log–log plot. This is done in an attempt to provide a qualitative basis for comparison with one of the predictions from the 'film drainage' analysis of Jones & Wilson (1978), namely that the film thickness should decrease at a rate proportional to t^{-m} where $m = \frac{1}{2}$ for a film between two solid surfaces, and $m = \frac{1}{3}$ for two free surfaces (zero tangential stress) in the absence of gravity (i.e. no hydrostatic pressure variations). Thus, if the film produced in the present theory were sufficiently thin, and if the quasi-static and other approximations of the Jones–Wilson analysis were valid, we should expect a final asymptotic slope between $-\frac{1}{3}$ and $-\frac{1}{2}$ for the results shown in figure 6. Unfortunately, though the final calculated slopes are definitely between 0 and -1 in most cases for $\lambda = 1$ and 10, we cannot make a stronger statement from the numerical results available. The slope for $\lambda = 0.1$ is definitely larger than -1, but it is doubtful whether the quasi-static approximation should apply to the 'fast-drainage' case, and this is seemingly corroborated by the fact that we never achieve the 'dimpled film' configuration in that case.

One important qualitative conclusion from the present results is that the 'dimpled film' configuration can be promoted (and thus coalescence inhibited) not only via surfactant immobilization of the interfaces, but also by decrease of the viscosity of the suspending fluid. It may be seen, upon closer examination of figure 6, that the

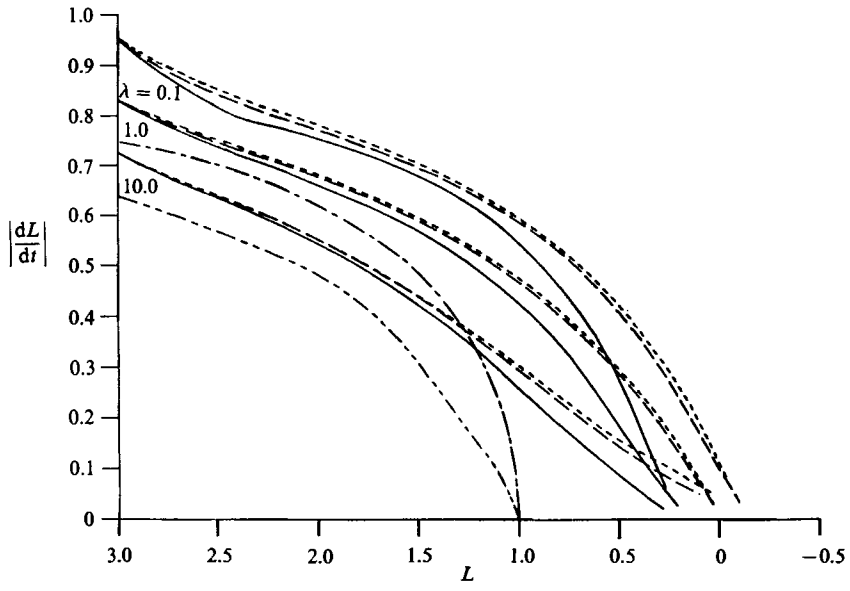

FIGURE 7. Dimensionless velocity of the centre of mass of the drop $|dL/dt|$, as a function of the dimensionless distance of the centre of mass of the drop from the undeformed flat surface, L; ——, $Ca = 0.2$; – – – –, $Ca = 1.0$; - - - -, $Ca = 10$. Also, — · —, solid sphere, non-deforming free interface; — · · —, solid sphere, solid wall.

variation in λ not only changes the relative rates of film drainage, but also exerts a strong influence on the 'quasi-asymptotic' film thicknesses that appears for large t. In particular, larger values of λ are not only associated with slower drainage but also larger 'asymptotic' film thickness, which again will tend to inhibit coalescence.

Finally, for completeness we show in figure 7, the dimensionless velocity of the centre of mass of the drop as it approaches the interface. Also shown for comparison is the velocity of a solid sphere approaching a solid wall, and a solid sphere approaching a non-deforming free surface with $\lambda = 0$, both taken from the analytical results of Brenner (1961). In all cases, i.e. for all λ and Ca, the drop velocity rapidly approaches zero as the centre of mass crosses the plane of the undeformed interface. However, this is only partially due to hydrodynamic interaction between the drop and the interface. Since the density of the drop and its homophase are equal, the driving force for motion goes rapidly to zero as $L \to 0$. However, for $L > 1.0$, the primary influence on drop velocity is the hydrodynamic interaction between the drop and the deforming interface. In all cases shown in figure 7, the velocity is non-dimensionalized so that it will approach unity for $L \to \infty$. Thus, for the drops, we use

$$u_c = U_\infty = \frac{2}{9}\frac{ga^2(\rho_2 - \rho_1)}{\mu_2}\frac{1}{\beta},$$

where

$$\beta = \left(1 + \frac{2}{3\lambda}\right)\Big/\left(1 + \frac{1}{\lambda}\right),$$

with the solid-sphere results corresponding to $\beta = 1 (\lambda \to \infty)$. Thus, all of the difference between the various results is a consequence of differences in the degree of hydrodynamic interaction between the drop and the interface. We see that the

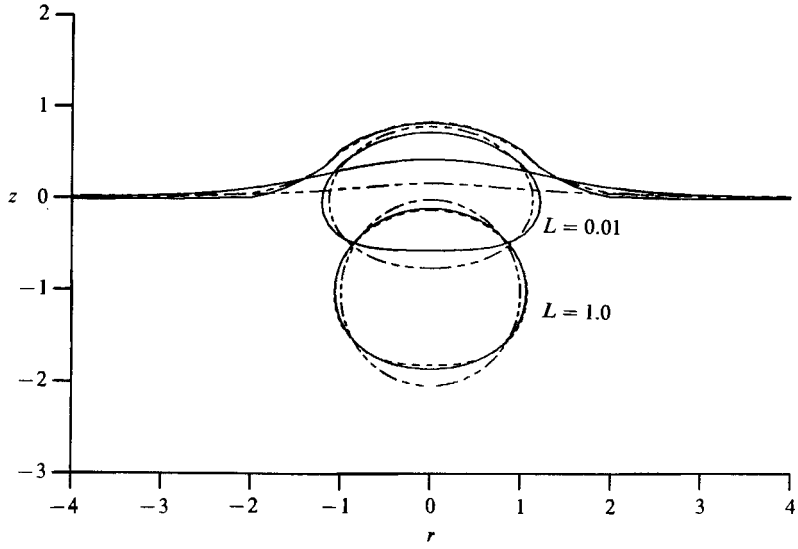

FIGURE 8. Shapes of the drop and the interface for $Ca = 2.0, \lambda = 0.5$; —·—·—, $L_{t=0} = 1.2$; ——, $L_{t=0} = 3$; - - - -, $L_{t=0} = 7$.

deformation of the drop and interface greatly reduces the magnitude of the 'wall effect', especially for the smaller values of λ, relative to that for a solid sphere. Of course, the solid sphere is geometrically constrained from passing across the plane $z = 0$, whereas the drop can do so, both because of interface deformation and because the drop flattens out, and this is a major contributor to the differences in results for $L \leqslant 1.0$. However, the weaker 'wall' effects for larger L are a consequence of modified hydrodynamic interaction, rather than simple geometric constraints. There are two main sources of the decreased magnitude of hydrodynamic interaction that is evident in figure 7. First, the interface is mobile, and thus moves in the same direction as the drop. Second, as it becomes deformed, it lies further from the drop for a given value of L than it would if it remained flat. In the cases considered here, it is primarily the first of these mechanisms that contributes to the weaker effect of the interface on the drop relative to the results shown for the sphere. To see that this is the case, we need only recall that the results for $L = 3$ are all for a flat interface and a spherical drop. The differences for various λ values at this point are therefore a reflection only of the increase in velocity of the interface away from the drop as λ is decreased.

The primary influence of Ca on drop velocity occurs for the smallest value, $Ca = 0.2$, and then primarily when the interface and drop become quite strongly deformed. At this point, the relatively strong capillary effect resists additional deformation and the very small drop velocity becomes primarily dependent upon Ca. The fact that there is no influence of Ca on the results for $L = 3$ is a consequence of the fact that the interface is flat at $t = 0$. Thus, initially, capillary forces play no role in its deformation. Capillary forces do play a role in the drop deformation from the initial spherical shape but this is apparently a minor effect for $L \sim 3$.

4.2. *The effect of initial configuration*

The initial configuration considered in all of the preceding results was a spherical drop initially situated with its centre at a distance $L_{t=0} = 3$ from a flat interface. This

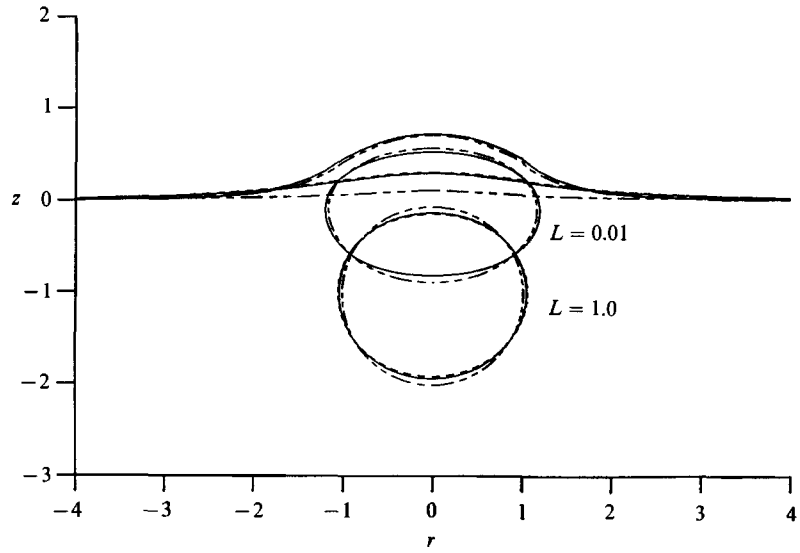

FIGURE 9. Shapes of the drop and the interface for $Ca = 2.0, \lambda = 10$; —·—·—, $L_{t=0} = 1.2$; ——, $L_{t=0} = 3$; ----, $L_{t=0} = 7$.

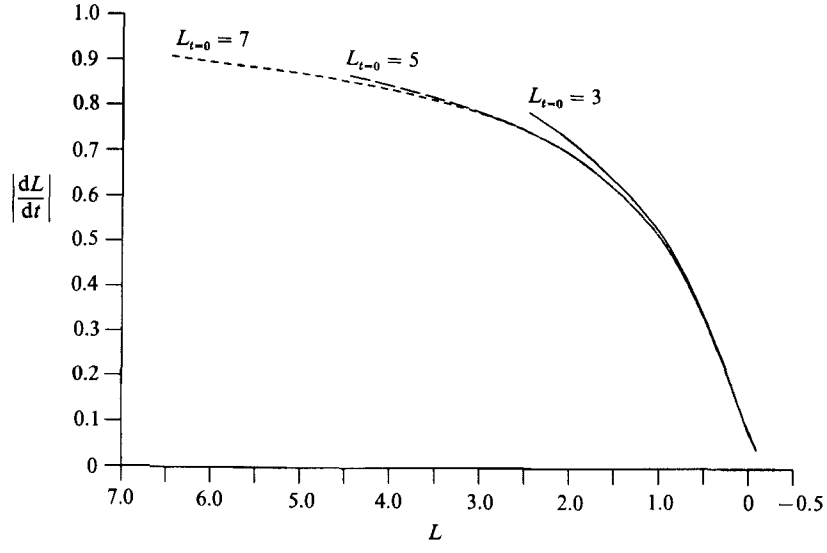

FIGURE 10. Dimensionless velocity of the centre of mass of the drop, $|dL/dt|$, as a function of the dimensionless distance of the centre of mass of the drop from the undeformed flat interface, L, for $Ca = 2.0, \lambda = 0.5$.

configuration was chosen as a compromise between the ideal of a very large initial distance between the drop and the interface, where the spherical drop and flat interfaces shapes are asymptotically exact, and the necessity for reasonable overall computation times. It is, of course, known that the solution of the problem (3)–(12) is strictly dependent upon initial conditions for all time. What is not known is the sensitivity of the solution to changes in initial conditions. To justify the choice $L_{t=0} = 3$, it is necessary to consider the effect of initial conditions on the interface and drop shapes and motion. It is to be hoped that the results for $L_{t=0} = 3$ are at least

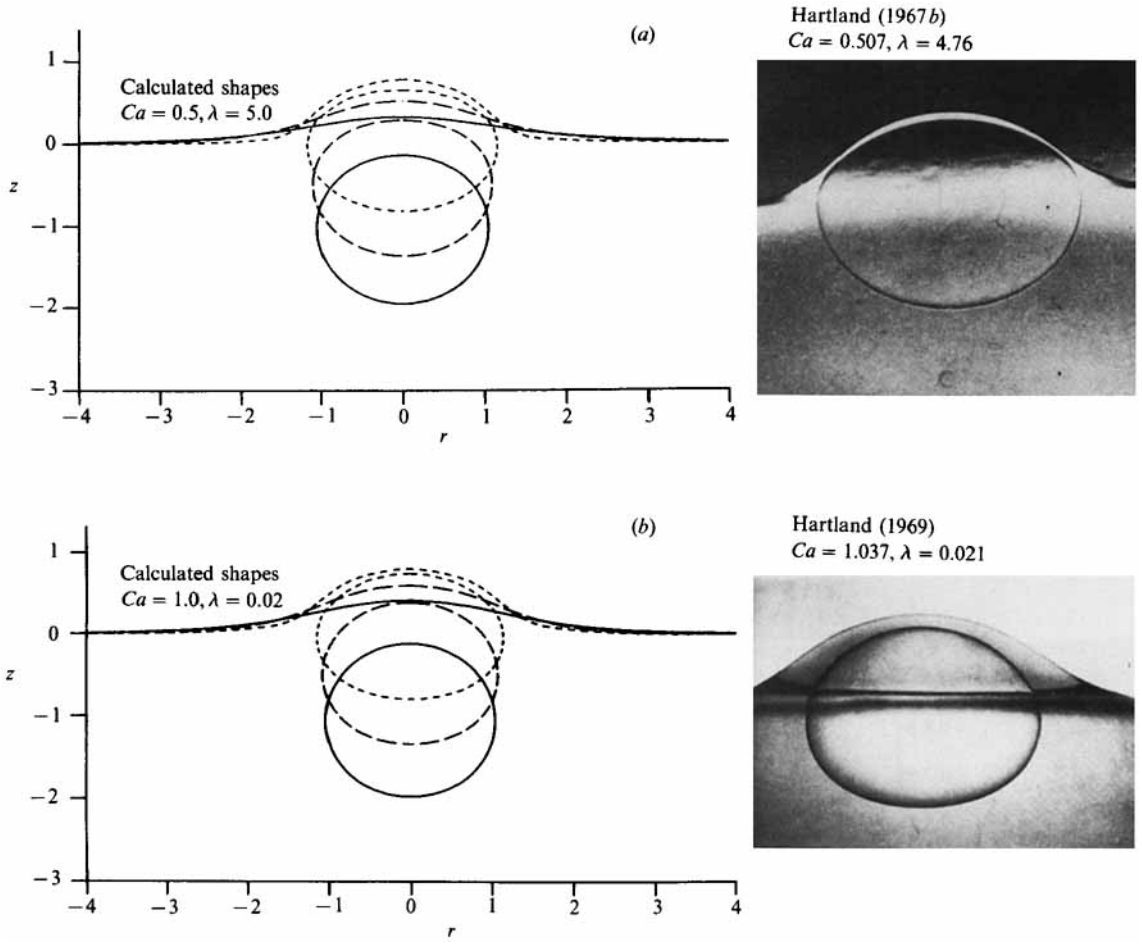

FIGURE 11. Comparison of the calculated shapes of the drop and the interface with the experimental photographs; ——, $L = 1.0$; – – – –, $L = 0.5$; - - - -, $L = 0.01$.

qualitatively representative of behaviour for a reasonably wide range of initial conditions. From a more general point of view, many experimental studies of film drainage have been initiated with the drop released very close to the interface and it is of interest to determine whether this initial configuration alters the film geometry in any fundamental way.

We consider two cases $Ca = 2.0, \lambda = 0.5$ and $Ca = 2.0, \lambda = 10$, each for three different initial positions of the drop, $L_{t=0} = 1.2$, 3 and 7, respectively. The shape of the drop and interface is shown in figures 8 and 9 for $L = 1.0$ and 0.01. It can be seen in both cases that the drop shapes at $L = 0.01$ become identical for the two initial positions, $L_{t=0} = 3$ and 7. However, for $L_{t=0} = 1.2$ the drop and interface shapes at $L = 0.001$ differ significantly from the shapes for $L_{t=0} = 3$ and 7, particularly for $\lambda = 0.5$. In this case, there is a qualitative change in the film profile from one with nearly constant thickness for $L_{t=0} \geqslant 3$, to a film of the 'rapid' drainage type which is very thin at the axis of symmetry for $L_{t=0} = 1.2$. Since the drop velocity is very small for $L = 0.01$ (cf. figure 7), and coalescence will occur primarily as a consequence of drainage from the thin film, this change in film geometry (especially the major

decrease in minimum film thickness) will produce important changes in the dynamics of the coalescence process. The sensitivity of the film geometry to the initial configuration displayed in figure 8 suggests that considerable care should be taken in the interpretation of experimental studies where the drop is started close to the interface.

Another indication that the results for $L_{t=0} = 3$ are representative of larger values of $L_{t=0}$ is shown in figure 10, where we plot the velocity of the centre of mass versus position for $Ca = 2.0, \lambda = 0.5$ and three initial configurations with $L_{t=0} = 3$, 5 and 7. As can be seen, the velocities become identical for all three cases for $L < 0.7$.

4.3. *Comparison with experimental results*

Calculations were carried out for two cases to compare present theoretical results with the previously published experimental results of Hartland (1967*b*, 1969). In figure 11, the shapes of the drop and interface for the two cases when $Ca = 0.5$, $\lambda = 5.0$ and $Ca = 1.0, \lambda = 0.02$ are compared with experimental photographs due to Hartland. In these experimental investigations, the drop was formed at the tip of a needle very close to the interface. Thus the drop was already deformed during the formation at the tip prior to release from the needle. However, current calculations were started with a spherical drop 3 radii away from a flat interface. Therefore, a quantitative comparison of the result would not be expected to add much to our understanding. However, our present results agree well, on a qualitative basis, with Hartland's results. Particularly, in figure 11(*b*) the film drains uniformly, while in figure 11(*a*) a 'dimple' occurs so that the film is thinnest in the region away from the central symmetry axis.

5. Conclusions

In this paper, we have studied the motion of a viscous deformable drop at low Reynolds number toward an initially flat fluid interface, for the special case in which the drop and the second bulk fluid are identical. Although many previous investigators have studied the same problem using film-drainage theories, these are usually limited to either no-slip (immobile interface) or zero tangential stress (mobile interface) conditions on the drop surface and the interface, and thus cannot reveal the effect of the bulk fluid properties inside the drop or in the second bulk fluid. Furthermore, such studies generally consider only the last stages of drop–interface interactions starting from an assumed initial film geometry. The present solutions are complementary to the film-drainage theories in the sense that they are numerically exact, starting with the drop at a large distance from the interface, and provide insight into the dependence of the initial film geometry on the capillary number and viscosity ratio.

The most significant result of our calculations is the fact that three distinct types of film geometry arise as a result of variations of the viscosity ratio between the drop (and the upper bulk fluid) and the lower bulk fluid, corresponding to three mechanisms of film drainage. For $\lambda = 0.1$, we find that 'rapid' drainage occurs, while 'uniform' drainage occurs for $\lambda = 1.0$. 'Dimpled' drainage, where the minimum film thickness appears at the rim, occurs for $\lambda = 10$. Similar drainage patterns were observed experimentally by Hodgson & Woods (1969) and Burrill & Woods (1973) by varying the concentration of surfactants. However, the current study illustrates that these different patterns can also arise for clean interfaces due solely to changes in the bulk viscosity ratio.

The majority of existing film-drainage theories, on the other hand, are basd upon a dimpled film configuration, either as an initial *ad hoc* assumption (cf. Lin & Slattery 1982) or as a consequence of a 'quasi-equilibrium' assumption (cf. Jones & Wilson 1978) in which pressure variations arise owing solely to hydrostatic and capillary effects. It is perhaps not surprising that the latter analysis seems to become increasingly relevant as λ increases, and that the 'quasi-equilibrium' approximation (with resultant 'dimpled film') does not seem to apply at all for $\lambda = 0.1$, even though $Re = 0$ for the range of film configurations considered. It is, of course, possible that the 'rapid draining' geometries obtained for the smaller λ will eventually revert to a dimpled film since velocities are becoming very small for $L \approx 0$, but if this occurs, it must only be relevant for much thinner films than those illustrated in figures 3–5. Whether such films can (or will) be achieved in reality depends on their stability, and thus on their thickness relative to the distance of action of van der Waals and other non-hydrodynamic forces, and is not a question that can be answered here.

Since the dimpled drainage pattern is intrinsically slower than drainage from a film with the minimum film thickness at the axis of symmetry, it may be advantageous to attempt to promote this mode if it is desired to minimize coalescence rates, or vice versa if rapid coalescence is desired. The present results indicate that the dimpled film configuration is unavoidable for viscous drops ($\lambda > 1$) independent of whether the interfaces are mobile or immobile. For less viscous drops ($\lambda \leqslant 1$), on the other hand, it may be possible to control the drainage mode through the level of surfactant that is present.

This work was supported by the fluid mechanics program of the National Science Foundation. The work was completed while L. G. Leal was a visitor in Chemical Engineering at the Massachusetts Institute of Technology. We wish to thank these institutions for support of this research.

Appendix

In the dimensional form, equation (11) is

$$\boldsymbol{n}_1 \cdot \boldsymbol{T}_2 - \boldsymbol{n}_1 \cdot \boldsymbol{T}_1 = \gamma_{12}(\nabla \cdot \boldsymbol{n}_1)\boldsymbol{I} \cdot \boldsymbol{n}_1 - (\rho_2 - \rho_1) gz\boldsymbol{I} \cdot \boldsymbol{n}_1. \tag{A 1}$$

Rearranging (A 1), we obtain

$$\boldsymbol{n}_1 \cdot \boldsymbol{T}_2 = \boldsymbol{n}_1 \cdot \boldsymbol{T}_1 + \gamma_{12}(\nabla \cdot \boldsymbol{n}_1)\boldsymbol{n}_1 - (\rho_2 - \rho_1) gz\boldsymbol{I} \cdot \boldsymbol{n}_1. \tag{A 2}$$

Then, the drag force on the drop is

$$\boldsymbol{F}_{\mathrm{D}} = \int \boldsymbol{n}_1 \cdot \boldsymbol{T}_2 \, \mathrm{d}S_{\mathrm{D}} = \int \boldsymbol{n} \cdot \boldsymbol{T}_1 \, \mathrm{d}S_{\mathrm{D}} + \int \gamma_{12}(\nabla \cdot \boldsymbol{n}_1)\boldsymbol{n}_1 \, \mathrm{d}S_{\mathrm{D}} - \int (\rho_2 - \rho_1) gz\boldsymbol{I} \cdot \boldsymbol{n}_1 \, \mathrm{d}S_{\mathrm{D}}. \tag{A 3}$$

Applying the divergence theorem to the first term of the right-hand side of (A 3), it can be shown that

$$\int \boldsymbol{n}_1 \cdot \boldsymbol{T}_1 \, \mathrm{d}S_{\mathrm{D}} = \int \nabla \cdot \boldsymbol{T}_1 \, \mathrm{d}V_{\mathrm{D}} = 0 \tag{A 4}$$

because

$$\nabla \cdot \boldsymbol{T}_1 = 0$$

for Stokes equations.

Now, consider the second term of the right-hand side (A 3). The surface divergence theorem states that for any scalar function ϕ on a surface S

$$\int \phi(\nabla \cdot \boldsymbol{n})\boldsymbol{n} \, \mathrm{d}S = \int \nabla\phi \, \mathrm{d}S - \oint_C \phi \boldsymbol{t} \, \mathrm{d}l, \tag{A 5}$$

where C denotes any closed curve on the surface S, and $\boldsymbol{t}$ denotes the unit vector that is normal to the curve C and tangent to the surface at each point. Then, by applying the surface divergence theorem, the second term of the right-hand side of (A 3) becomes

$$\int \gamma_{12}(\boldsymbol{\nabla}\cdot\boldsymbol{n}_1)\,\boldsymbol{n}_1\,\mathrm{d}S_{\mathrm{D}} = \int \boldsymbol{\nabla}\gamma_{12}\,\mathrm{d}S_{\mathrm{D}} - \oint \gamma_{12}\,\boldsymbol{t}\,\mathrm{d}l. \tag{A 6}$$

The first term of the right-hand side of (A 6) is zero because $\boldsymbol{\nabla}\gamma_{12} = 0$ for constant γ_{12}. And the second term of the right-hand side of (A 6) is zero because

$$\oint_C \gamma_{12}\,\boldsymbol{t}\,\mathrm{d}l = 0$$

for a closed volume. Finally, applying the divergence theorem to the third term on the right-hand side of (A 3),

$$-\int (\rho_2-\rho_1)\,gz\boldsymbol{I}\cdot\boldsymbol{n}_1\,\mathrm{d}S_{\mathrm{D}} = -(\rho_2-\rho_1)\,g\int \boldsymbol{\nabla}\cdot z\boldsymbol{I}\,\mathrm{d}V_{\mathrm{D}}. \tag{A 7}$$

The right-hand side of (A 7) is then

$$-(\rho_2-\rho_1)\,g\boldsymbol{i}_z\int \mathrm{d}V_{\mathrm{D}} = -(\rho_2-\rho_1)\,g\boldsymbol{i}_z\tfrac{4}{3}\pi a^3, \tag{A 8}$$

where a is the undeformed drop radius. Thus, the third term of the right-hand side of (A 3) is just the buoyancy force acting on the drop. Combining (A 3), (A 4), (A 5), and (A 8), we therefore see that a solution of the creeping motion which satisfies the stress boundary conditions (A 1) automatically satisfies a macroscopic force balance on the drop, in which the hydrodynamic force $\boldsymbol{F}_{\mathrm{D}}$ is just balanced by the buoyancy force.

REFERENCES

Allen, R. S., Charles, G. E. & Mason, S. G. 1961 The approach of gas bubbles to a gas/liquid interface. *J. Colloid Interface Sci.* **16**, 150.

Brenner, H. 1961 The slow motion of a sphere through a viscous fluid toward a plane surface. *Chem. Engng Sci.* **16**, 242.

Burrill, K. A. & Woods, D. R. 1969 Change in interface and film shapes for a deformable drop at a deformable liquid–liquid interface. *J. Colloid Interface Sci.* **30**, 511.

Burrill, K. A. & Woods, D. R. 1973 Film shapes for deformable drops at liquid–liquid interfaces. II. The mechanism of film drainage. *J. Colloid Interface Sci.* **42**, 15.

Charles, G. E. & Mason, S. G. 1960 The coalescence of liquid drops with flat liquid–liquid interfaces. *J. Colloid Interface Sci.* **15**, 236.

Chen, J. D., Hahn, P. S. & Slattery, J. C. 1984 Coalescence time for a small drop or bubble at a fluid–fluid interface. *AIChE J.* **30**, 622.

Frankel, S. P. & Mysels, K. J. 1962 On the 'dimpling' during the approach of two interfaces. *J. Phys. Chem.* **66**, 190.

Geller, A. W., Lee, S. H. & Leal, L. G. 1986 The creeping motion of a spherical particle toward a deformable interface. *J. Fluid Mech.* **169**, 27.

Hahn, P. S. & Slattery, J. C. 1985 Effects of surface viscosities on the stability of a draining plane parallel liquid film as a small bubble approaches a liquid–gas interface. *AIChE J.* **31**, 950.

Hahn, P. S. & Slattery, J. C. 1986 Effects of surface viscosities on the thinning and rupture of a dimpled liquid film as a small bubble approaches a liquid–gas interface. *AIChE Symposium Series. No.* 252, vol. 82, p. 100.

Hartland, S. 1967*a* The coalescence of a liquid drop at a liquid–liquid interface. Part I: Drop shape. *Trans. Inst. Chem. Engrs* **45**, T97.

HARTLAND, S. 1967*b* The coalescence of a liquid drop at a liquid–liquid interface. Part II: Film thickness. *Trans. Inst. Chem. Engrs* **45**, T102.

HARTLAND, S. 1967*c* The coalescence of a liquid drop at a liquid–liquid interface. Part III: Film rupture. *Trans. Inst. Chem. Engrs* **45**, T109.

HARTLAND, S. 1967*d* The coalescence of a liquid drop at a liquid–liquid interface. Part V: The effect of surface active agents. *Trans. Inst. Chem. Engrs* **45**, T275.

HARTLAND, S. 1969 The effect of circulation patterns on the drainage of the film between a liquid drop and a deformable liquid–liquid interface. *Chem. Engng Sci.* **24**, 611.

HARTLAND, S. 1970 The profile of the draining film between a fluid drop and deformable fluid–liquid interface. *Chem. Engng J.* **1**, 67.

HODGSON, T. D. & WOODS, D. R. 1969 The effect of surfactants on the coalescence of a drop at an interface. II. *J. Colloid Interface Sci.* **30**, 429.

JONES, A. F. & WILSON, S. D. R. 1978 The film drainage problem in drop coalescence. *J. Fluid Mech.* **87**, 263.

LADYZHENSKAYA, O. A. 1963 *The Mathematical Theory of Viscous Incompressible Flow.* Gordon and Breech.

LEE, S. H. & LEAL, L. G. 1982 Motion of a sphere in the presence of a deformable interface. Part 2: Numerical study of the translation of a sphere normal to an interface. *J. Colloid Interface Sci.* **87**, 81.

LIN, C. Y. & SLATTERY, J. C. 1982 Thinning of a liquid film as a small drop or bubble approaches a fluid–fluid interface. *AIChE J.* **28**, 786.

MACKAY, G. D. M. & MASON, S. G. 1963 The gravity approach and coalescence of fluid drops at liquid interfaces. *Can. J. Chem. Engng* **41**, 203.

PRINCEN, H. M. 1963 Shape of a fluid drop at a liquid–liquid interface. *J. Colloid Interface Sci.* **18**, 178.

PRINCEN, H. M. & MASON, S. G. 1965 Shape of a fluid drop at a fluid–fluid interface. I. Extension and test of two-phase theory. *J. Colloid Interface Sci.* **29**, 156.

REED, X. B., RIOLO, E. & HARTLAND, S. 1974*a* The effect of hydrodynamic coupling on the axisymmetric drainage of thin films. *Intl J. Multiphase Flow* **1**, 411.

REED, X. B., RIOLO, E. & HARTLAND, S. 1974*b* The effect of hydrodynamic coupling on the thinning of a film between a drop and its homophase. *Intl J. Multiphase Flow* **1**, 437.

RIOLO, E., REED, X. B. & HARTLAND, S. 1975 The effect of hydrodynamic coupling on the steady drainage of a thin film between a solid sphere approach a fluid–fluid interface. *J. Colloid Interface Sci.* **50**, 49.

YOUNGREN, G. K. & ACRIVOS, A. 1976 On the shape of a gas bubble in a viscous extensional flow. *J. Fluid Mech.* **76**, 433.